A Periodic DFT Study of Isobutene Chemisorption in Proton-Exchanged Zeolites: Dependence of Reactivity on the Zeolite Framework Structure

Xavier Rozanska,* Rutger A. van Santen,* Thomas Demuth,† François Hutschka,‡ and Juergen Hafner†

Schuit Institute of Catalysis, Laboratory of Inorganic Chemistry and Catalysis, Eindhoven University of Technology, P.O. Box 513, NL5600MB Eindhoven, The Netherlands, Totalfinaelf, Raffinerie des Flandres, Département Technique, Secteur Technique no 4, BP 79, F59279 Loon Plage, France, and Institut für Materialphysik, Universität Wien, Sensengasse 8, A1090 Wien, Austria

Received: July 18, 2002; In Final Form: December 10, 2002

Isobutene chemisorption within proton-exchanged zeolites is investigated using periodic density functional theory method. This allows us to consider the effect of the zeolite micropore dimension to reactivity. The isobutene reaction pathways that proceed through primary and tertiary carbocation-like transition states have been investigated. The results agree with predicted reactivity trends. Activation energies of isobutene chemisorption are estimated to be around 100 and 25 kJ/mol for primary and tertiary transition states, respectively. Destabilization of transition state complexes and products are as observed before. Interestingly, because of the steric constraints, the chemisorbed alkoxy species appeared to become as unstable as protonated hydrocarbons. The more significant result is the correlation of the zeolite micropore dimension with activation energies. Fluctuations of the activation energies are observed as a function of the match of the transition state structures with the zeolite cavities. We define a limit to the applicability of the semiempirical Polaniy−Evans−Brønsted relation in zeolite catalysis.

Introduction

One of the main aims of petrochemical industry is the transformation of crude petrol into gas oil and gasoline.[1] For this purpose, cracking, isomerization, and hydrogenation processes are employed. Commonly used catalyst components for these processes are the zeolites.[1,2] Used at large scale in petrochemistry since the 1960s,[3] zeolite or zeolite-based catalysts are especially relevant because of the unique properties of the zeolite crystals. Zeolite crystals show good mechanical and thermal stability.[1−4] They have also a very high microporous surface area[5] and well-identified structures. The micropore network induces selectivity[5] effects as it can lead to selective diffusion of reactants and products[5,6] and to selective formation of transition states.[5,7] Last, zeolites are environmentally friendly catalysts, because they are solid catalyst. Heterogeneous catalysts are advantageous since they avoid costly separation processes of products and catalyst part, which produce large amount of waste.[1−2,8]

However, environmental regulations put some constraints on the composition of gas oil and gasoline. Especially, to minimize toxicity of exhaust gases, the content in aromatics has been and will be further decreased.[9] A direct consequence of the lower concentration of aromatics in transportation fuel is the reduction of the octane number.[10] A solution fortunately exists to compensate for this, before alternatives solutions, such as the gas-powered or electrical vehicles, take over the traditional hydrocarbon combustion.[9,10] The conversion of short linear alkane into branched alkane produces fuels with an acceptable octane number.[9] This isomerization is achieved by using bifunctional catalysts, which consist there of small metallic clusters, viz. Pt, Pd, or Ru, dispersed within an acidic zeolite catalyst.[3b,11,12] The main steps of the corresponding bifunctional reaction are summarized in Scheme 1.

In this reaction, alkane is dehydrogenated into olefin, which is then isomerized. Hydrogenation of isomerized olefin follows. The dehydrogenation and hydrogenation are catalyzed by the metallic catalyst part, whereas the isomerization of alkene is catalyzed by the acidic zeolite catalyst.[3b,12] Optimization of metal loading of the catalysts results in isomerization of the olefin to be the rate-limiting step.[12] Prior to this reaction, olefin has to chemisorb to the acid zeolite catalytic site.[13] Therefore, an understanding of the reactivity of chemisorbed olefin is important. It may help to predict which isomerization reaction pathway will most likely be followed. Many studies have been performed to identify this reaction pathway.[1−5,9−12] However, strong debates still today exist on the details.[14]

In this study, we will focus on the reactivity of proton-exchanged zeolites. Let us more deeply describe some of the properties of zeolites and zeolite catalysts. We mentioned that zeolites are aluminosilicates. They are insulator materials, characterized with close-to-vacuum dielectric constant.[15] Polarization of zeolitic oxygen atoms induces long-range electrostatic contributions to play a rather limited role.[7,16−18] The interaction between a guest molecule and the zeolite framework is dominated by short-range electrostatic contributions.[17] Acid zeolite catalysts can be generated when a framework silicon atom is substituted with an aluminum atom. Then, a cation is introduced to neutralize the negative charge.[18] The nature of the cation is important, as zeolites are commonly employed in

* To whom correspondence should be addressed. Fax +31 40 245 5054. E-mail: tgakxr@chem.tue.nl.
† Institut für Materialphysik.
‡ Centre Européen de Recherche et Technique, Totalfinaelf.

10.1021/jp021646b CCC: $25.00
Published on Web 01/21/2003

SCHEME 1: Isomerization of Alkane Catalyzed by a Bifunctional Catalyst[1,2]

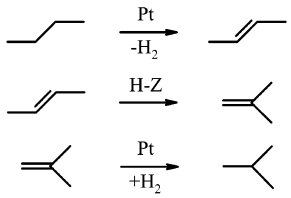

ion-exchanged processes.[19] Zeolitic acid Brønsted sites are obtained when the zeolites are proton-exchanged.

Acidic zeolites are able to catalyze hydrocarbon reactions similar as those obtained with superacids.[3b,20] However, since the pioneering studies of Kazansky et al.[13a] and Haw et al.,[13b] it is well-understood that proton-exchanged zeolites are actually moderate acids, and that carbocations can usually only exist within the zeolite microporous structure as transient species. On the other hand, acid zeolite reactivity has clearly been identified to involve carbocationic transition states.[1−14] As acid zeolites are only moderately acidic, the selectivity of reaction is very sensitive with respect to carbocation type, viz. primary, secondary, and tertiary, implicated in the transition state structure.[3b,12,18b]

Because short-range electrostatic contributions dominate in the interactions between the zeolite framework and the carbocationic transition state complexes, the transition state energetics strongly depend on the zeolite topology of the neighboring atoms of the catalytic site. This has been demonstrated in several theoretical studies. Sauer et al.[21] have shown how important is the topology of zeolite in hydrogen-jump around the Brønsted site. Sinclair et al.[22] performed an analysis of olefin chemisorption within proton-exchanged chabazite. They analyzed the dependence of reactivity on match of the hydrocarbon molecule size and micropore structure using an embedding procedure. Vos et al.[7] achieved a study of the alkylation of toluene with methanol in acidic mordenite. This study constitutes a good illustration of transition state selectivity in zeolite. Also, we recently described in a study of isomerization of toluene and xylenes catalyzed by acidic mordenite, how important is the zeolite topology in the selection of reaction pathways.[23]

An important feature that controls reactivity is local zeolite elasticity. It has been shown that the local flexibility of a zeolite crystal varies. Kramer et al.[24] and Catlow et al.[25] analyzed the changes in the topology of zeolite framework when defects, such as Brønsted sites, are introduced. They observed that the zeolite framework became only locally affected in this process. However, the amount of deformation depends strongly on the type of reaction. It has been demonstrated that electron delocalization is crucial in helping transition state stabilization.[23,26] Induced dipoles on the zeolitic oxygen atoms contribute to the stabilization of carbocationic transition state. Then, a correct description of zeolite framework elasticity is mandatory to analyze this effect, as induced dipoles and electron delocalization change slightly but significantly the zeolite framework atom positions.[27] This deformation is shape-dependent with the zeolite framework and transition state complex topologies.

The zeolite crystal long-range electrostatic contributions has been shown to play a nonnegligible part in differences in stabilization energies of carbocationic transition states.[21a,28] Because the transition state molecular structure has a net positive charge, the Coulombic interactions within the system are enhanced and therefore must be accurately described.[29] The Madelung constant of the zeolite crystal has been used in some

SCHEME 2: Reaction Mechanisms in the Chemisorption of Isobutene Catalyzed by Acidic Zeolite

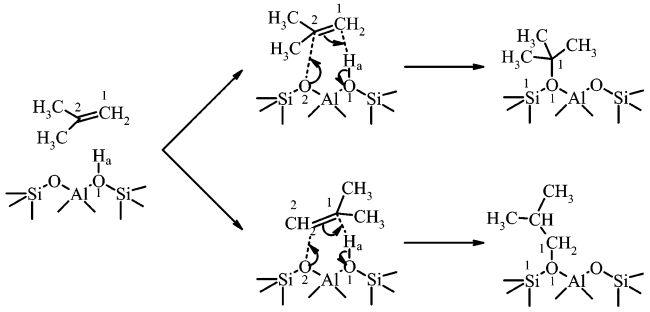

studies to correct cluster computed transition state energies.[16,30] Such corrected activation energies appeared to be in relatively good qualitative agreement with experimental data, be it overestimated as the zeolite framework is inaccurately modeled.

In this study, we will analyze chemisorption of isobutene in different acidic zeolites (see Scheme 2). This will help to understand zeolite structural difference effects on butane isomerization. Moreover, isobutene is the smallest hydrocarbon molecule for which tertiary carbocation-like transition states can be formed. We considered the case of propylene chemisorption in chabazite in a previous study.[27] With propylene, only primary and secondary carbocation-like transition states could be investigated. To analyze the effect of zeolite framework on isobutene chemisorption, chemisorption in chabazite (CHA),[30] ZSM-22 (TON),[32] and mordenite (MOR)[33] zeolites will be considered.[34] For the purpose of this study, we will use the periodic density functional theory (DFT) program VASP.[35] The quantum chemistry periodic method constitutes a convenient method to study zeolite reactivity, as it allows a realistic description of the zeolite framework.[7,23,27,36]

Methods

VASP was used to perform all calculations.[35] The total energy is obtained by solving the Kohn−Sham equations of the local density approximation (LDA) with the Perdew−Zunger exchange-correlation functional.[37] The results are corrected for nonlocality within the generalized gradient approximation (GGA) with the Perdew-Wang 91 functional.[38] VASP uses plane-waves basis set and pseudopotentials.[39]

A cutoff energy of 400 eV was used. Brillouin zone sampling was restricted to the Γ-point. A quasi-Newton forces-minimization algorithm was employed for the calculations. Physisorbed isobutene and alkoxides were optimized using a conjugate-gradient algorithm after forces were decreased below 0.10 eV/Å using the quasi-Newton forces-minimization algorithm. Convergence was assumed to be achieved when forces were below 0.05 eV/Å.

The transition state (TS) search method in VASP is the nudged elastic band (NEB) method.[40] Several images of the system are defined along the investigated reaction pathway. These images are optimized by allowing a relaxation in the subspace perpendicular to the reaction coordinate.

Up to four images were used to investigate reaction pathways in the NEB calculations. When all forces in the intermediate states fall below 0.08 eV/Å, the system with the highest energy in the reaction pathway was separately optimized using a forces minimization.

Analysis of isobutene protonation was carried out in three different zeolite crystals. Optimization of the unit cells was achieved in the absence of isobutene following the procedure

TABLE 1: Main Geometrical Parameters of Physisorbed Isobutene in H-CHA, H-TON, and H-MOR as Obtained in the Periodic DFT Calculations[a]

	CHA	TON	MOR
AlO_1	1.90	1.89	1.90
O_1H_a	1.01	1.03	1.02
H_aC_1	2.00	1.99	1.98
H_aC_2	2.70	2.13	2.45

[a] All data in angstroms. Labels are defined in Scheme 2.

as previously employed.[7,27] Next, size and shape of the unit cells was maintained constant. We shown that this has a little effect on energies as well as geometries of the systems in a previous study.[27]

The dimensions of the unit cells are $a = 9.246$ Å, $b = 9.273$ Å, $c = 9.264$ Å, $\alpha = 94.3°$, $\beta = 93.9°$, and $\gamma = 93.5°$; $a = 11.169$ Å, $b = 11.123$ Å, $c = 15.113$ Å, $\alpha = 90.0°$, $\beta = 90.2°$, and $\gamma = 77.2°$; and $a = 13.648$ Å, $b = 13.672$ Å, $c = 15.205$ Å, $\alpha = 96.8°$, $\beta = 90.0°$, and $\gamma = 90.0°$ for H-CHA, H-TON, and H-MOR, respectively. Optimization and description of CHA and MOR unit cells using VASP has been extensively described in previous studies.[36]

Further verifications were achieved in the chemisorbed olefin systems. Because of the complexity of the potential energy surface, it was easy to get as optimized structures local minima in these systems. All structures were checked using dynamic annealing simulations.[41] The simulations ran over 600 dynamic steps with a time step of 1 fs, in NVT conditions. The temperature was linearly decreased every 10 steps from 800 K in the beginning to 10 K in the end of the simulation. To avoid alkoxide to desorb from the zeolite wall when the kinetic energy of the system was high, the position of the C−O alkoxy bond was maintained during the dynamic simulations. The geometries that were eventually obtained after these annealing simulations were again optimized and compared to the initial ground states.

Results

Many theoretical studies have been achieved on olefin chemisorption in acidic zeolite.[22,42] In these studies, the catalytic site was modeled as a small cluster fragment terminated with hydrogen atoms. This method known as the cluster approach method does not aim to model the zeolite framework in an accurate way but focuses on the zeolite catalytic site. Recent progress in computer technology allows nowadays calculations of realistic zeolitic models.[7,23,27,36,41]

It is well-described that olefin physisorbed to the acid Brønsted site of a zeolite crystal is not a very stable situation. Olefin is readily protonated.[42] However, because charge separation is energetically costly in acidic zeolite,[18b] olefin does not exist as free carbocation. At the same time that olefin protonation occurs, an alkoxy bond between a carbon atom of the olefin and an oxygen atom of the zeolite catalytic site is formed so as to stabilize the positive charge.

The protonation−chemisorption of isobutene can lead to two different products (see Scheme 2).

Isobutene adopts an η^2(CC) adsorption mode in contact to the zeolitic proton. Main geometrical parameters of isobutene physisorbed to the Brønsted acidic site in the three different zeolite unit cells are summarized in Table 1. In all the cases, the physisorbtion of C═C of isobutene to the proton leads to a weakening of the O−H bond. The OH bond stretches from 0.99 to 1.01−1.03 Å in olefin physisorbtion. The proton points at a nontotally equidistant position of the C═C bond, being closer to C_1 than to C_2 (see Table 1).

In the transition states, the O_1-H_a bond is broken, whereas H_a jumps to a carbon atom of the C═C bond, leading to the formation of a C−H bond.[17,22,42] At the same time, a positive charge is induced on the carbon atom next to the one that is protonated.[42] This induced positive charge will only exist during the transition state structure, because the loss of the acidic proton in the zeolite catalytic site generates a negative charge on the zeolite framework. The excess of electron density on the catalytic site is important to the formation of an alkoxy bond between the zeolite surface and the hydrocarbon molecule. The main geometry parameters in the transition state complexes that lead to the formation of isobutoxide or *n*-butoxide in the three different zeolites are summarized in Table 2. One notes that in all transition state complexes, the O_1H_a bond is already clearly broken (O_1H_a between 1.30 and 1.85 Å), whereas the bond between the olefin carbon atom and the proton is not yet completely formed (H_aC_1 between 1.14 and 1.37 Å).

As can be seen in Table 2, the zeolite oxygen atom, the proton, and the carbon atom are located along an almost straight line in every transition states. The angle that is formed by $C_1C_2O_2$ is close to 90° in all TS. There is no really noticeable difference for the characteristic angles in the TS structures whatever is the product.

Concerning the distances between the atoms that are involved in the alkoxy bond, the situation is different whether *i*-butoxide or *n*-butoxide is the product. C_2O_2 is around 2.5 Å in case *n*-butoxide will be formed, whereas it is around 3.2 Å in isobutoxide formation. This is explained by the relative stability of the carbocations being involved in the transition state complexes. Upon protonation of isobutene, a primary or a tertiary carbocation-like transition state structure can be formed. It is known that the primary carbocation is much less stable than tertiary carbocation.[1] The lower stability of the primary carbocation-like transition state tends to be compensated by a closer interaction with the negatively charged zeolitic catalytic site. In case of the tertiary carbocation-like transition state, this interaction is much less pronounced, and the transition state structure is closer to a free carbocationic structure.[22,30,42]

Study of isobutene chemisorption to zeolite Brønsted site has been done before using the cluster approach by Rigby and Frash[42] and Sinclair et al.[22] They reported some geometry parameters in the transition states (see Table 2). One notes that exactly the same geometry trends are obtained in the cluster approach results as in the periodic electronic structure calculation results. However, as indicated before by Vollmer and Truong[30] in an embedded cluster study of hydrogen exchange of methane with H-zeolite Y, the explicit presence of the zeolite framework increases the carbocationic nature of the transition state. This is also observed here in Table 2: the protonated hydrocarbon is always closer to the Brønsted acidic site in the cluster approach calculations than in the periodic calculations.

Let us now analyze the geometries of the alkoxy species. Alkoxy distances are rather different whether the alkoxy species is isobutoxide or *n*-butoxide. This is a significant result in the analysis of the geometries of the alkoxy species in the three different zeolite crystals (see Table 3). As indicated by the C−O bond distance, the isobutoxy C−O bond is weaker than that of *n*-butoxide. Similar trends were observed by Rigby and Frash.[42] This result is explained by the electronic inductive effect of the methyl groups connected to the carbon atom. It stabilizes more the positive charge on the carbon atom that is involved in the alkoxy bond.[42] Next, the orientation of the alkoxide with respect to the zeolite catalytic site does not seem to follow any

TABLE 2: Main Geometrical Parameters of the Transition States in the Chemisorption of Isobutene as Obtained in Theoretical Calculations[a]

zeolite TS[b]	CHA *n*	CHA *i*	TON *n*	TON *i*	MOR *n*	MOR *i*	cluster[c] *n*	cluster[c] *i*	cluster[c] *i*
source							[42]	[42]	[22]
AlO_1	1.78	1.75	1.78	1.82	1.81	1.83			
AlO_2	1.73	1.73	1.74	1.72	1.73	1.70			
O_1H_a	1.61	1.85	1.69	1.30	1.48	1.35	1.29	1.41	1.40
H_aC_1	1.25	1.14	1.26	1.37	1.29	1.33	1.31	1.23	1.31
C_1C_2	1.39	1.43	1.39	1.38	1.39	1.39	1.39	1.41	1.39
C_2O_2	2.45	3.06	2.52	3.26	2.46	3.28	2.08	2.45	3.37
$O_1H_aC_1$	172.6	168.2	167.1	172.0	175.1	172.1			
$C_1C_2O_2$	107.9	86.6	117.1	98.0	107.3	96.1			

[a] Angles in degrees, distances in angstroms. Labels are defined in Scheme 2. [b] *n* for TS that leads to the formation of *n*-butoxide, and *i* for TS that leads to the formation of *i*-butoxide. [c] A zeolitic molecular fragment was used to model the zeolite catalyst in these studies.

TABLE 3: Main Geometrical Parameters of Chemisorbed Isobutene in CHA, TON, and MOR as Obtained in the Periodic DFT Calculations[a]

zeolite species[b]	CHA *n*	CHA *i*	TON *n*	TON *i*	MOR *n*	MOR *i*
AlO_1	1.88	1.88	1.90	1.92	1.88	1.90
O_1Si_1	1.69	1.69	1.69	1.71	1.69	1.69
O_1C_1	1.52	1.64	1.52	1.65	1.52	1.64
AlO_1Si_1	125.8	121.0	127.6	118.8	131.7	124.5
AlO_1C_1	110.6	119.4	114.3	119.4	114.4	117.3
$AlO_1Si_1C_1$	164.4	172.6	173.4	−173.2	178.9	175.1

[a] Angles in degree, distances in angstroms. Labels are defined in Scheme 2. [b] *n* for *n*-butoxide, and *i* for *i*-butoxide.

TABLE 4: Computed Energy Parameters for Isobutene Chemisorption in CHA, TON, and MOR as Obtained in the Periodic DFT Calculations[a]

zeolite	E_{act}[b] *n*	E_{act}[b] *i*	ΔE[c]	$\Delta E_{\sigma-\pi}$[d] *n*	$\Delta E_{\sigma-\pi}$[d] *i*
CHA	138	45	43	10	43
TON	90	24	23	−28	18
MOR	118	30	25	2	3

[a] In kJ/mol. All energies are with respect to the corresponding physisorbed isobutene. [b] Activation energies to *n*-butoxide (*n*) and *i*-butoxide (*i*). [c] Energy difference between physisorbed isobutene and *i*-butyl tertiary carbocation state. [d] Energy difference between *n*-butoxide (*n*) or *i*-butoxide (*i*) and physisorbed isobutene.

general trend, and it is rather controlled by the overall local topology of the zeolite framework (see Table 3).

The activation energies of the chemisorption of isobutene in H-CHA, H-TON, and H-MOR are presented in Table 4. In all the cases, reaction that proceeds to *n*-butoxide seems very unlikely to occur as E_{act} is on the order of ∼120 kJ/mol. Reaction follows readily transformation through tertiary carbocation-like transition state complex, as such a step has an activation energy of the order of $E_{act} \sim 30$ kJ/mol.

The same energy ordering with respect to the type of intermediate carbocation was also observed in a periodic DFT study of propylene chemisorption[27] and in cluster approach calculations.[42] One should mention that E_{act} in chemisorption through the primary carbocation-like TS of isobutene is similar to that of propylene primary carbocation-like TS.[27]

Discussion

Common features of isobutene chemisorption within H−CHA, H-TON, and H-MOR have been described in the previous section. Now, we will discuss differences induced by the zeolite frameworks.

We observed in previous periodic DFT studies of reactions catalyzed by acidic zeolite that the zeolite framework has a significant impact on stabilizing carbocationic transition states complexes.[7,23,44−46] The importance of the interactions between the zeolite framework and TS complexes was clearly revealed when periodic results were confronted to cluster approach results. We used in our cluster approach studies of reaction catalyzed by acidic zeolite catalytic sites rather small cluster models.[7,45,46] The advantage of following this approach is that we were able to follow the reaction in the absence of any zeolite framework dependence. We observed that for a given size of transition state complexes and a given zeolite structure, the effect of the zeolite could be estimated as constant.[7,23,44−46] A strong stabilization of TS complexes in interaction with the zeolite micropore was obtained in our calculations in comparison with cluster approach calculations.[7,23,27,44−46] We identified that zeolite oxygen atoms were playing an important role in this stabilization.[23,27] The carbocationic TS complexes induced dipoles on the zeolitic oxygen atoms.[23,27]

Zeolite crystal long-range electrostatic contributions to the stabilization of carbocations are known to be of limited importance.[13,19b] However, zeolitic oxygens can easily be polarized. The interaction of hydrocarbon molecules with the zeolite micropore is dominated by short-range electrostatic contribution.[18,26]

This was nicely illustrated by Besuz et al.[47] In their attempt to define force field parameters to describe the interaction of alkanes with the zeolite framework, they ended up with a very elegant formulation in which silicon atoms were not considered, but extra terms to take into account polarization of oxygen atoms had to be included.

Ramanchandran et al.[26b] observed also in a theoretical study of hydrocarbon cracking within acidic zeolite that short range electrostatic contributions and especially induced charges and electron delocalization were of importance in the interaction between TS complexes and the zeolite framework.

In case short-range electrostatic contributions are important in the stabilization of carbocationic TS, one should find direct evidence of differences in activation energy of reaction catalyzed by zeolites with different micropore structures.

Let us describe the different zeolites that were used in the periodic electronic structure calculations.[34] MOR is a large pore zeolite (see Figure 1a). It has parallel 12-membered rings in which isobutene is not expected to experience any steric constraints. Furthermore, the Brønsted acidic site that was selected in the calculations was located at the junction of a 12-membered ring and two smaller eight-membered rings.[7,23,44] Therefore, alkoxy species are not expected to suffer from steric constraints. TON is a medium size micropore zeolite: it has parallel 10-membered ring channels without side pockets or openings of any sort in the channels (see Figure 1b). CHA micropore structure consists of supercages connected to each others through eight-membered ring openings (see Figure 1c).

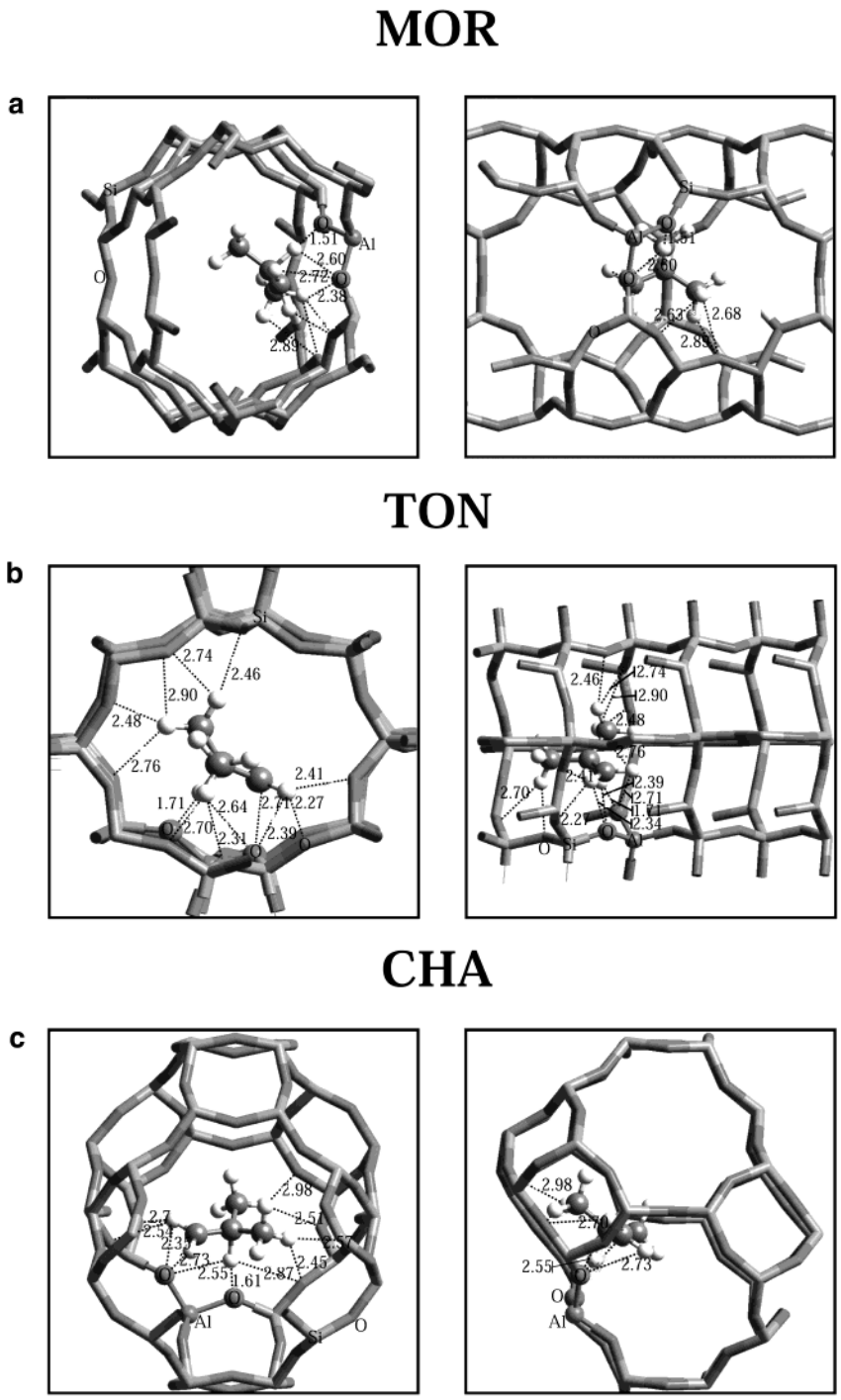

Figure 1. Transition states that lead to the formation of *n*-butoxide in MOR (a), TON (b), and CHA (c). Distances between isobutene H atoms and zeolite O atoms are reported.

So, beside CHA has "large" cavities, the curvature of the zeolite wall has a radius that is smaller to that of in TON.

As expected, primary carbocation like transition states present much higher activation energies than tertiary carbocation-like transition states (see Table 4). It is well-known from experimental data of reactions catalyzed by acidic zeolites that activation energies follow the same ordering as the carbocation type intermediates.[1] This explains why carbocation related intermediates are often depicted in the experimental description of reaction pathways.[1−3] Protonation to tertiary carbocation structures occurs readily whatever is the zeolite structure, with activation energy on the order of 24−45 kJ/mol. One notes that the energy of the tertiary carbocation intermediate is very close to that of the corresponding transition state (see Table 4).

The geometries of the transition states that lead to the formation of *n*-butoxide are shown in Figure 1. Distances between zeolite oxygen atoms and isobutene hydrogen atoms in the range 0−3 Å are reported in the three zeolite catalysts. One notes that in TON, in which the activation energy is the lower, the match between the size of the transition state structure and the zeolite micropore size is ideal. This is not the case in CHA and MOR: in these zeolites, the oxygen atoms located to the opposite side of the micropore to which the reaction occurs are more than 3 Å away from the TS complex.

Similar activation energy trend is observed in tertiary carbocation-like transition states, be it less pronounced.

In case of no steric constraints (i.e., in MOR), the relative energies of the alkoxy species are expected and found to be the

same for the isobutoxy and *n*-butoxy species. This differs in CHA and TON. In these zeolites, the curvature of the zeolite surface induces steric constraints that destabilize the more bulky *i*-butoxy species. In CHA, *n*-butoxy species are also destabilized. One notes that the absence of contact between the alkoxy species and the zeolite wall does not help much in stabilizing their energies: linear butoxide in TON is more stable than in MOR.

A striking result is that *i*-butoxide in CHA and TON becomes as stable as the free tertiary carbocation. The contribution of steric constraints to the destabilization of TS complex is not observed in TON, whereas it is in CHA. This explains why the activation energies of *i*-butoxy and *n*-butoxy species are higher in CHA in comparison to that of in TON and MOR (see Table 4). We previously analyzed steric constraints effect to activation energies and observed that the Polaniy−Evans−Brønsted relation could be used to estimate TS structure destabilization.[7,23,44,46]

One can apply the Polaniy−Evans−Brønsted relation[41,46,48] to get further insights in the data. This relation is based on semiempirical results[48] and was also observed to be valid in theoretical DFT studies.[41,46,49] It was observed that adsorption energy fluctuations induced linear variations of activation energy for a given reaction under similar conditions. Previously, we applied this relation to reactions catalyzed by zeolite in quantum chemical studies.[41] We observed that the Polaniy−Evans−Brønsted relation was useful and reasonably accurate to estimate zeolite steric constraints effect on reactions.

The relative activation energy and adsorption energy differences for the isobutene activation in zeolites are shown in Table 4. If the Polaniy−Evans−Brønsted relation is valid, reaction energy differences and activation energy differences should be linearly dependent. One can see that this is indeed not the case. This result is, however, predictable.

As previously discussed, zeolite framework stabilizes carbocationic transition state structures. This stabilization is mainly caused by short-range electrostatic interactions between the zeolitic oxygen atoms and the transition state structures. In the present study, the zeolite frameworks are very different from CHA, TON, and to MOR zeolites. Therefore, the interactions between the zeolite framework and TS structures differ (see Figure 1), as also do the stabilization energies of TS structures by the zeolite frameworks. However, the interaction of neutral species (viz., physisorbed isobutene and covalently bonded alkoxides) with the zeolite framework is not of same nature as the one in transition state structures. In the first case, van der Waals energy contributions dominate, whereas in the later case it is short-range electrostatic contributions. Differences in transition state complex energy stabilization with respect to the size of the zeolite cage cannot be estimated from the energy variation of reactant or product. Hence, the Polaniy−Evans−Brønsted relation is unsuccessful in this case. However, it can still be used to estimate the effect of the zeolite steric constraints as the nature of the energy destabilization is the same for reactant, transition state complex and product.[41] Then, using this partial Polaniy−Evans−Brønsted relation,[48b] one can estimate that the activation energies for *n*-butoxide formation in absence of steric constraints should be around 90, 100, and 120 kJ/mol in TON, MOR, and CHA, respectively. In *i*-butoxide formation, the predicted activation energies in absence of steric constraints should be around 20, 25, and 30 kJ/mol in TON, CHA, and MOR, respectively.

The relative stabilization of the transition state structure in case of good match between the size of the transition state and that of the zeolite framework is not surprising as it is dominated by short-range electrostatic contribution. Large micropores stabilize TS relatively little. Too small, a micropore induces steric constraints that destabilize the TS. The ideally sized micropore is the one for which TS complex has the best fit with the micropore. The results presented here confirm that short-range electronic contributions are a significant driving force in the stabilization of TS structures.

Conclusions

An important result that has been obtained in this study is the fact that *i*-butoxide is not always formed. In fact, the TS to *i*-butoxide formation, the *i*-butyl tertiary carbocation, and *i*-butoxide energy levels may become very close to each other, when steric constraints influence the shape of the reaction potential energy surface (see Table 4). The details critically depend on the zeolite catalyst structure.

An estimation of activation energies in the proton-exchanged zeolite catalyst in relation to the carbocationic nature of the transition state is given. The activation energies are around 25, 60, or 110 kJ/mol for TS complexes that are tertiary, secondary, or primary carbocation-like, respectively.[27] For transition states that involve a methenium carbocation, the activation energy is around 180 kJ/mol.[23,44]

However, these numbers do not account for other contributions that have been shown to subtly or crudely affect this ordering. These contributions are related to (i) zeolite micropore shape and (ii) to the chemical nature of the system. The second point is rather obvious: the above-mentioned results are valid for hydrocarbons and cannot be generalized to other systems.

Transition state selectivity in zeolites has been already analyzed and described in other studies.[7,12,23,41,44,46] We observed in these studies,[12,27,46] and in agreement with literature[13,15,26,43,47] that short-range electrostatic contributions are important to the stabilization of the carbocationic-like TS. The systematic study of isobutene in different structures of zeolite allowed us to analyze the dependence of TS stabilization in relation with zeolite micropore size. It is found that activation energy is smallest in case of optimum fit of the TS complex shape with zeolite micropore size. The differences in activation energies found are around 20 kJ/mol for an activation energy of the order of 110 kJ/mol in absence of steric constraints. Such energy differences are highly sufficient to induce reaction pathway selectivity. In the tertiary carbocation-like TS, the relative energy difference is proportionally similar (i.e., of the order of ∼20% of the activation energy). However, the activation energies for this step are around 25 kJ/mol in absence of steric constraints.

Finally, we observe that the limit of applicability of the Polaniy-Evans-Brønsted is reached in this system. The semiempirical relation is not universal but can be applied in case the nature of the interactions between reactants, transition state complexes, and products and the catalyst is the same. A partial form of the relation is very useful to get further insight into the zeolitic steric constraints effect in reaction.[41,46]

Acknowledgment. Computational resources were partly granted by the Dutch National Computer Facilities (NCF). This work was performed within the European Research Group "Ab Initio Molecular Dynamics Applied to Catalysis", supported by CNRS, IFP, and Totalfinaelf. X. R. thanks Totalfinaelf for the financial support.

References and Notes

(1) (a) Jacobs, P. A.; Martens, J. A. *Introduction to Zeolite Science and Practice*; Van Bekum, H., Flaningen, E. M., Jansen, J. C., Eds.;

Elsevier: Amsterdam, 1991; pp 445−496. (b) Maxwell, I. E.; Stork, W. H. J. *Introduction to Zeolite Science and Practice*; Van Bekum, H., Flaningen, E. M., Jansen, J. C., Eds.; Elsevier: Amsterdam, 1991; pp 571−630.

(2) Venuto, P. B. *Microporous Mater*. **1994**, *2*, 297−411.

(3) (a) Thomas, J. M.; Thomas, W. J. *Principles and Practice of Heterogeneous Catalysis*; VCH: Weinheim, 1997; pp 6−10. (b) Martens, J. A.; Jacobs, P. A. *Handbook of Heterogeneous Catalysis*; G. Ertl, H. Knözinger; J. Weitkamp, Eds.; VCH: Weinheim, 1997; pp 1137−1149.

(4) (a) Thomas, J. M.; Thomas, W. J. *Principles and Practice of Heterogeneous Catalysis*; VCH: Weinheim, 1997; pp 257−318. (b) Van Santen, R. A.; Niemantsverdriet, J. W. *Chemical Kinetics and Catalysis*; Plenum Press: New York, 1995; pp 89−102.

(5) (a) Csicsery, S. M. *Zeolites* **1984**, *4*, 202−213. (b) Fraenkel, D.; Levy, M. *J. Catal*. **1989**, *118*, 10−21. (c) Chen, N. Y., Degnan, T. F., Jr., Smith, C. M., Eds. *Molecular Transport and Reaction in Zeolites, Design and Application of Shape Selective Catalyst*; VCH Publishers: New York, 1994; pp 195−289. (d) Tsai, T.-C.; Liu, S.-B.; Wang, I. *Appl. Catal. A* **1999**, *181*, 355−398.

(6) (a) Keil, F. J.; Krishna, R.; Coppens, M.-O. *Rev. Chem. Eng*. **2000**, *16*, 71−197. (b) Schuring, D.; Jansen, A. P. J.; Van Santen, R. A. *J. Phys. Chem. B* **2000**, *104*, 941−948. (c) Schuring, D.; Koriabkina, A. O.; De Jong, A. M.; Smit. B.; Van Santen, R. A. *J. Phys. Chem. B* **2001**, *105*, 7690−7698. (d) Smit, B.; Siepmann, J. I. *J. Phys. Chem.* **1994**, *98*, 8442−8452. (e) Smit, B. *Mol. Phys.* **1995**, *85*, 153−172. (f) Smit, B.; Maesen, T. L. M. *Nature* **1995**, *374*, 42−44. (g) Deka, R. C.; Vetrivel, R.; Miyamoto, A. *Top. Catal.* **1999**, *9*, 225−234. (h) Yang, L.; Trafford, K.; Kresnawahjuesa, O.; Sepa, J.; Gorte, R. J. *J. Phys. Chem. B* 2001, 105, 1935−1942.

(7) Vos, A. M.; Rozanska, X.; Schoonheydt, R. A.; Van Santen, R. A.; Hutschka, H.; Hafner, J. *J. Am. Chem. Soc*. **2001**, *123*, 2799−2809.

(8) Farcasiu, D. *Catal. Lett.* **2001**, *71*, 95−103.

(9) Marcilly, C. *Zeolites and Mesoporous Materials at the Dawn of the 21st Century*; A. Galarneau, A., F. Di Renzo, F. Fajula, J. Vedrine, Eds.; Studies in Surface Science Catalysis 135; Elsevier: Amsterdam, 2001; pp 37−60.

(10) Chica, A.; Corma, A.; Miguel, P. J. *Catal. Today* **2001**, *65*, 101−110.

(11) (a) Van de Runstraat, A.; Van Grondelle, J.; Van Santen, R. A. *Ind. Eng. Chem. Res*. **1997**, *36*, 3116−3125. (b) Van de Runstraat, A.; Kamp, J. A.; Stobbelaar, P. J.; Van Grondelle, J.; Krijnen, S.; Van Santen, R. A. *J. Catal*. **1997**, *171*, 77−84.

(12) Van Santen, R. A.; Rozanska, X. *Molecular Modeling and Theory in Chemical Engineering*; Wei, J., Seinfeld, J. H., Denn, M. M., Stephanopoulos, G., Chakraborty, A., Ying, J., Peppas, N., Eds.; Advances in Chemical Engineering 28; Academic Press: New York, 2001; pp 399−437.

(13) (a) Kazansky, V. B.; Senchenya, I. N. *J. Catal*. **1989**, *119*, 108−120. (b) Haw, J. F.; Richardson, B. R.; Oshiro, I. S.; Lazo, N. D.; Speed, J. A. *J. Am. Chem. Soc.* **1989**, *111*, 2052−2058. (c) Haw, J. F.; Nicholas, J. B.; Xu, T.; Beck, L. W.; Ferguson, D. B. *Acc. Chem. Res.* **1996**, *29*, 259−267.

(14) (a) Kondo, J. N.; Yoda, E.; Wakabayashi, F.; Domen, K. *Catal. Today* **2000**, *63*, 305−308. (b) Ivanov, P.; Papp, H. *Langmuir* **2000**, *16*, 7769−7772. (c) Domokos, L.; Lefferts, L.; Seshan, K.; Lercher, J. A. *J. Mol. Catal. A* **2000**, *162*, 147−157. (d) Rutenbeck, D.; Papp, H.; Freude, D.; Schwieger, W. *Appl. Catal. A* **2001**, *206*, 57−66. (e) Rutenbeck, D.; Papp, H.; Ernst, H.; Schwieger, W. *Appl. Catal. A* **2001**, *208*, 153−161. (f) Patrigeon, A.; Benazzi, E.; Travers, Ch.; Bernhard, J. Y. *Catal. Today* **2001**, *65*, 149−155. (g) Philippou, A.; Dwyer, J.; Ghanbari, A.; Pazè, C.; Anderson, M. W. *J. Mol. Catal. A* **2001**, *174*, 223−230. (h) Patrylak, K. I.; Bobonych, F. M.; Voloshyna, Yu. G.; Levchuck, M. M.; Solomakha, V. M.; Patrylak, L. K.; Manza, I. A.; Taranookha, O. M. *Catal. Today* **2001**, 65, 129−135.

(15) (a) De Man, A. J. M.; Van Beest, B. M. W.; Leslie, M.; Van Santen, R. A. *J. Phys. Chem.* **1990**, *94*, 2524−2534. (b) Schröder, K.-P.; Sauer, J. *J. Phys. Chem.* **1996**, *100*, 11043−11049.

(16) Zygmunt, S. A.; Curtiss, L. A.; Zapol, P.; Iton, L. E. *J. Phys. Chem. B* **2000**, *104*, 1944−1949.

(17) Zhen, S.; Seff, K. *Microporous Mesoporous Mater*. **2000**, *39*, 1−18.

(18) (a) Bell, R. G.; Jackson, R. A.; Catlow C. R. A. *Zeolites*, **1992**, *12*, 870−871. (b) Van Santen, R. A.; Kramer, G. J. *Chem. Rev.* **1995**, *3*, 637−660. (c) Fricke, R.; Kosslick, H.; Lischke, G.; Richter, M. *Chem. Rev*. **2000**, *100*, 2303−2405.

(19) (a) Barrer, R. M. *Zeolite and Clay Minerals as Sorbents and Molecular Sieves*; Academic Press: New York, 1978; pp 1−22. (b) Sárkány, J. *Appl. Catal. A* **1999**, *188*, 369−379. (c) Vayssilov, G. N.; Rösch, N. *J. Phys. Chem. B* **2001**, *105*, 4277−4284. (d) Sponer, J. E.; Sobalík, Z.; Leszczynski, J.; Wichterlová, B. *J. Phys. Chem. B* **2001**, *105*, 8285−8290.

(20) (a) Olah, G. A.; Donovan, D. J. *J. Am. Chem. Soc*. **1977**, *99*, 5026−5039. (b) Olah, G. A.; Prakash, G. K. S.; Sommer, J. *Superacids*; Wiley-Interscience: New York, 1985. (c) Olah, G. A.; Prakash, G. K. S.; Williams, R. E.; Field, L. D.; Wade, K. *Hypercarbon Chemistry*; Wiley-Interscience: New York, 1987.

(21) (a) Sauer, J.; Sierka, M.; Haase, F. *Transition State Modeling for Catalysis*; Truhlar, D. G., Morokuma, K., Eds.; ACS Symposium Series 721; American Chemical Society: Washington, DC, 1999; pp 358−367. (b) Sierka, M.; Sauer, J. *J. Phys. Chem. B* **2001**, *105*, 1603−1613.

(22) Sinclair, P. E.; De Vries, A.; Sherwood, P.; Catlow, C. R. A.; Van Santen, R. A. *J. Chem. Soc., Faraday Trans.* **1998**, *94*, 3401−3408.

(23) Rozanska, X.; Van Santen, R. A.; Hutschka, F.; Hafner, J. *J. Am. Chem. Soc*. **2001**, *123*, 7655−7667.

(24) Kramer, G. J.; De Man, A. J. M.; Van Santen, R. A. *J. Am. Chem. Soc.* **1991**, *113*, 6435−6441.

(25) (a) Catlow, C. R. A.; Ackermann, L.; Bell, R. G.; Gay, D. H.; Holt, S.; Lewis, D. W.; Nygren, M. A.; Sastre, G.; Sayle, D. C.; Sinclair, P. E. *J. Mol. Catal. A* **1997**, *115*, 431−448. (b) Willock, D. J.; Price, S. L.; Leslie, M.; Catlow, C. R. A. *J. Comput. Chem.* **1995**, *16*, 628−647.

(26) (a) Hammonds, K. D.; Deng, H.; Heine, V.; Dove, M. T. *Phys. Rev. Lett*. **1997**, *78*, 3701−3704. (b) Ramachandran, S.; Lenz, T. G.; Skiff, W. M.; Rappé, A. K. *J. Phys. Chem.* **1996**, *100*, 5898−5907.

(27) Rozanska, X.; Demuth, Th.; Hutschka, F.; Hafner, J.; Van Santen, R. A. *J. Phys. Chem. B* **2002**, *106*, 3248−3254.

(28) Boronat, M.; Zicovich-Wilson, C. M.; Corma, A.; Viruela, P. *Phys. Chem. Chem. Phys*. **1999**, *1*, 537−543.

(29) (a) Makov, G.; Payne, M. C. *Phys. Rev. B* **1995**, *51*, 4014−4022. (b) Rozanska, X.; Chipot, C. *J. Chem. Phys*. **2000**, *112*, 9691−9694. (c) Allen, M. P.; Tildesley, D. J. *Computer Simulation of Liquids*; Oxford Science Publications: New York, 1987; pp 155−166

(30) Vollmer, J. M.; Truong, T. N. *J. Phys. Chem. B* **2000**, *104*, 6308−6312.

(31) (a) Dent, L. S.; Smith, J. V. *Nature* **1958**, *181*, 1794−1796. (b) Feng, P. Y.; Bu, X. H.; Stucky, G. D. *Nature* **1997**, *388*, 735−741.

(32) (a) Barri, S. A. I.; Smith, G. W.; White, D.; Young, D. *Nature* **1984**, *312*, 533−534. (b) Highcock, R. M.; Smith, G. W.; Wood, D. *Acta Crystallogr*. **1985**, *C41*, 1391−1394.

(33) (a) Meier, W. M. *Z. Kristallogr*. **1961**, *115*, 439−450. (b) Eapen, M. J.; Reddy, K. S. N.; Joshi, P. N.; Shiralkar, V. P. *J. Inclusion Phenom*. **1992**, *14*, 119−129.

(34) Baerlocher, Ch.; Meier, W. M.; Olson, D. H. *Atlas of Zeolite Framework Types*, 5th ed.; Elsevier: Amsterdam, 2001.

(35) (a) Kresse, G.; Hafner, J. *Phys. Rev. B* **1993**, *48*, 13115−13126. (b) Kresse, G.; Hafner, J. *Phys. Rev. B* **1994**, *49*, 14251−14269. (c) Kresse, G.; Furthmüller, J. *Comput. Matter. Sci.* **1996**, *6*, 15−50. (d) Kresse, G.; Furthmüller, J. *Phys. Rev. B* **1996**, *54*, 11169−11186.

(36) (a) Jeanvoine, Y.; Àngyàn, J.; Kresse, G.; Hafner, J. *J. Phys. Chem. B* **1998**, *102*, 5573−5580. (b) Jeanvoine, Y.; Àngyàn, J.; Kresse, G.; Hafner, J. *J. Phys. Chem. B* **1998**, *102*, 7307−7310. (c) Benco, L.; Demuth, T.; Hafner, J.; Hutschka, F. *J. Chem. Phys.* **1999**, *111*, 7537−7545. (d) Benco, L.; Demuth, T.; Hafner, J.; Hutschka, F. *Chem. Phys. Lett.* **2000**, *324*, 373−380. (e) Demuth, T.; Hafner, J.; Benco, L.; Toulhoat, H. *J. Phys. Chem. B* **2000**, *104*, 4593−4607. (f) Benco, L.; Demuth, T.; Hafner, J.; Hutschka, F.; Toulhoat, H. *J. Chem. Phys.* **2001**, *114*, 6327−6334. (g) Demuth, T.; Benco, L.; Hafner, J.; Toulhoat, H.; Hutschka, F. *J. Chem. Phys* **2001**, *114*, 3703−3712.

(37) Perdew, J. P.; Zunger, A. *Phys. Rev. B* **1981**, *23*, 5048−5079.

(38) Perdew, J. P.; Burke, K.; Wang, Y. *Phys. Rev. B* **1996**, *54*, 16533−16539.

(39) Kresse, G.; Hafner, J. *J. Phys. Condens. Matter* **1994**, *6*, 8245−8257.

(40) Mills, G.; Jónsson, H.; Schenter, G. K. *Surf. Sci.* **1995**, *324*, 305−337.

(41) Rozanska, X.; Van Santen, R. A.; Hutschka, F. *J. Phys. Chem. B* **2002**, *41*, 4652−4657.

(42) Rigby, A. M.; Frash, M. V. *J. Mol. Catal. A* **1997**, *126*, 61−72.

(43) (a) Paukshtis, E. A.; Malysheva, L. V.; Stepanov, V. G. *React. Kinet. Catal. Lett*. **1998**, *65*, 145−152. (b) Derouane, E. G.; He, H.; Hamid, S. B. D.-A.; Ivanova, I. I. *Catal. Lett.* **1999**, *58*, 1−18.

(44) Rozanska, X.; Van Santen, R. A.; Hutschka, F.; Hafner, J. *J. Catal*. **2002**, *205*, 388−397.

(45) Rozanska, X.; Saintigny, X.; Van Santen, R. A.; Hutschka, F. *J. Catal*. **2001**, *202*, 141−155.

(46) Rozanska, X.; Van Santen, R. A.; Hutschka, F. *Theoretical Aspects of Heterogeneous Catalysis*; Nascimento, M. A. C., Ed.; Kluwer Academic Publishers: Norwell, MA, 2001; pp 1−28.

(47) (a) Bezuz, A. A.; Kiselev, A. G.; Loptakin, A. A.; Quang Du, P. *J. Chem. Soc., Faraday Trans. 2* **1978**, *74*, 367−379. (b) Bezuz, A. A.; Kocirik, M.; Kiselev, A. V.; Loptakin, A. A.; Vasilyena, E. A. *Zeolites* **1986**, *6*, 101−106.

(48) (a) Brønsted, N. *Chem. Rev*. **1928**, *5*, 231−338. (b) Evans, M. G.; Polaniy, N. P. *Trans. Faraday Soc*. **1938**, *34*, 11−29.

(49) Logadottir, A.; Rod, T. H.; Nørskov, J. K.; Hammer, B.; Dahl, S.; Jacobsen, C. J. H. *J. Catal*. **2001**, *197*, 229−231.